CHEMISTRY OF MATERIALS
Article

Chem. Mater. **2010,** *22,* 4987–4995 4987
DOI:10.1021/cm101263p

Displacive Ordering Transitions in Perovskite-Like $AgNb_{1/2}Ta_{1/2}O_3$

I. Levin,*[,†] J. C. Woicik,[†] A. Llobet,[‡] M. G. Tucker,[§] V. Krayzman, J. Pokorny,[⊥,∥] and I. M. Reaney[⊥]

[†]*Ceramics Division, National Institute of Standards and Technology, Gaithersburg Md 20899,* [‡]*Lujan Neutron Center, Los Alamos National Laboratory Los Alamos, NM,* [§]*ISIS, Rutherford Appleton Laboratory, Didcot, U.K.,* [⊥]*Department of Engineering Materials, University of Sheffield, Sheffield, U.K., and* [∥]*Institute of Physics, Academy of Sciences of the Czech Republic, Prague, Czech Republic*

Received May 5, 2010. Revised Manuscript Received June 29, 2010

Displacive phase transitions in perovskite-like solid solutions $AgNb_{1/2}Ta_{1/2}O_3$ were studied using several diffraction and spectroscopic techniques sensitive to average and local structures. The room-temperature phase of $AgNb_{1/2}Ta_{1/2}O_3$ (M_2) is analogous to that of the end-member $AgNbO_3$ and exhibits *Pbcm* orthorhombic symmetry with lattice parameters $\sqrt{2}a_c \times \sqrt{2}a_c \times 4a_c$ ($a_c \approx 4$ Å refers to an ideal cubic perovskite cell). This structure combines complex octahedral tilting and average antipolar B-cation (Nb, Ta) displacements. Similar to $AgNbO_3$, at higher temperatures, B-cations are disordered among multiple sites displaced along $\langle 111 \rangle_c$ directions. Partial ordering of local B-cation displacements is manifested in the so-called $M_3 \leftrightarrow M_2$ transition, which preserves the average *Pbcm* symmetry determined by the tilted octahedral framework; the transition is accompanied by a broad exploitable maximum of dielectric constant. Ta substitution suppresses this ordering because of the dissimilar off-centering trends for Ta and Nb. According to the extended X-ray absorption fine structure (EXAFS) measurements, Nb cations exhibit much larger local off-center displacements than Ta, consistent with larger dielectric constants typically displayed by niobates compared to tantalates. $AgNb_{1/2}Ta_{1/2}O_3$ maintains residual 8-site disorder down to low temperatures as opposed to 2-site disorder in $AgNbO_3$. Our results suggest that Ag cations also exhibit displacive disorder and, on cooling, undergo ordering coupled to that of the B-cations.

Introduction

$Ag(Nb,Ta)O_3$ perovskite-like solid solutions stand out among other dielectric ceramics because of their unique combination of large, temperature-stable dielectric constants and moderate dielectric losses at microwave (> 1 GHz) frequencies.[1,2] These remarkable properties have been attributed to a high-frequency dielectric relaxation associated with Nb dynamics which yields a broad peak in the temperature dependence of the dielectric constant.[3,4] The end-member compound $AgNbO_3$ exhibits a complex sequence of displacive polymorphic transitions on cooling from the high-temperature cubic phase (Figure 1).[5] These transitions involve changes in the types of octahedral tilting and cation (Ag, Nb) displacements.[5,6] The transition that coincides with a diffuse maximum of dielectric constant occurs between the so-called M_3 and M_2 structures at 275 °C. All the M-structures exhibit orthorhombic *Pbcm* symmetry and $\sqrt{2}a_c \times \sqrt{2}a_c \times 4a_c$ unit cells ($a_c \approx 4$ Å refers to an ideal cubic perovskite cell) defined by complex octahedral tilting (Figure 2).[6,7] The $M_3 \leftrightarrow M_2$ transition is manifested in an abrupt splitting of the 004_c (subscript c refers to an ideal cubic perovskite cell) reflection with no detectable changes in the space group symmetry.[5−7]

Our recent studies of the $M_3 \leftrightarrow M_2$ transition in $AgNbO_3$ using a combination of several diffraction and spectroscopic techniques concluded that it reflects long-range ordering of local $\langle 111 \rangle_c$ Nb displacements into an anti-polar-like array within the *Pbcm* symmetry of the tilted octahedral framework.[7] Complete ordering of Nb displacements is incompatible with this symmetry, and some residual 2-site Nb disorder is retained, as inferred from the presence of diffuse scattering sheets in electron diffraction.[7] $AgNbO_3$ and $AgTaO_3$, the latter of which crystallizes with a rhombohedral *R3c* structure featuring $a^-a^-a^-$ tilting,[8] form complete perovskite-like solid solutions. Ta substitution for Nb has little effect on the C ↔ T, T ↔ O, and O ↔ M transitions (Figure 1), all caused by

*To whom correspondence should be addressed. E-mail: igor.levin@nist.gov.

(1) Valant, M.; Suvorov, D.; Hoffmann, C.; Sommariva, H. *J. Eur. Ceram. Soc.* **2001**, *21*(15), 2647–2651.
(2) Valant, M.; Axelsson, A. K.; Alford, N. *J. Eur. Ceram. Soc.* **2007**, *27*(7), 2549–2560.
(3) Fortin, W.; Kugel, G. E.; Grigas, J.; Kania, A. *J. Appl. Phys.* **1996**, *79*(8), 4273–4282.
(4) Petzelt, J.; Kamba, S.; Buixaderas, E.; Bovtun, V.; Zikmund, Z.; Kania, A.; Koukal, V.; Pokorny, J.; Polivka, J.; Pashkov, V.; Komandin, G.; Volkov, A. *Ferroelectrics* **1999**, *223*, 235.
(5) Pawelczyk, M. *Phase Transitions* **1987**, *8*(4), 273–292.
(6) Sciau, P.; Kania, A.; Dkhil, B.; Suard, E.; Ratuszna, A.; Phys., J. *Condens. Matter* **2004**, *16*(16), 2795–2810.
(7) Levin, I.; Krayzman, V.; Woicik, J. C.; Karapetrova, J.; Proffen, Th.; Tucker, M. G.; Reaney, I. M. *Phys. Rev. B.* **2009**, *79*(10), 104113.
(8) Wolcyrz, M.; Lukaszewski, M. *Z. Kristallogr.* **1986**, *177*(1−2), 53–58.

Published on Web 08/05/2010

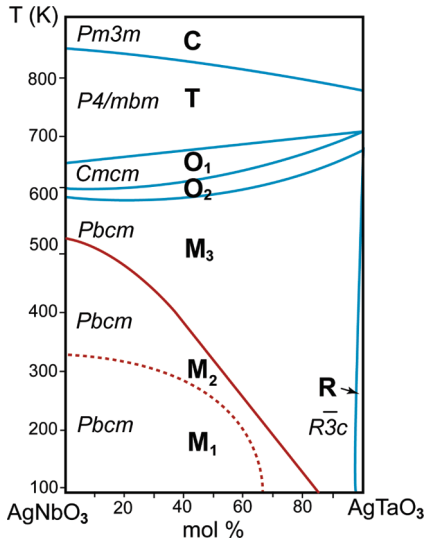

Figure 1. $AgNbO_3$–$AgTaO_3$ phase diagram (redrawn from ref 5).

octahedral tilting,[5] but suppresses the $M_3 \leftrightarrow M_2$ transition down to room temperature for $AgNb_{1/2}Ta_{1/2}O_3$. A broad dielectric peak associated with the $M_3 \leftrightarrow M_2$ transition is retained in $AgNb_{1/2}Ta_{1/2}O_3$, yielding the combination of a large dielectric constant and acceptable microwave losses in a practical temperature range.[1,2] In the present work, we extended our previous study of the phase transitions in $AgNbO_3$ to the industrially relevant $AgNb_{1/2}Ta_{1/2}O_3$ composition. Local- and average-structure sensitive diffraction and spectroscopic techniques were combined to elucidate the differences in the displacive behavior of Nb and Ta and their resulting effects on the phase transitions in this system. Since pentavalent Nb and Ta exhibit similar nominal ionic radii (~0.64 Å),[9] the $Ag(Nb,Ta)O_3$ system is devoid of atomic size-mismatch effects that often dominate the structural behavior of solid solutions. The dielectric data available for various Nb- and Ta-based oxide compounds consistently indicate a higher ionic polarizability for Nb.[10−12] Thus, studies of local structure in the $Ag(Nb,Ta)O_3$ system were expected to clarify the origins of different ionic polarizabilities observed for the two chemically analogous cations.

Experimental Section

$AgNb_{1/2}Ta_{1/2}O_3$ samples were prepared using a two-step solid-state synthesis. First, stoichiometric amounts of Nb_2O_5 (99.9985%) and Ta_2O_5 (99.993%) were mixed under acetone using an agate mortar and pestle, dried, pressed into pellets, and subjected to multiple heat treatments at 1450 °C (with intermediate grindings) for a total of 2 weeks. Equilibrium was assumed from the lack of significant changes in the X-ray line broadening. The resulting finely ground $(Nb,Ta)_2O_5$ powders were mixed with Ag_2O (cyclic permutation grade) by grinding under acetone, dried, pressed into pellets, and annealed two times (with intermediate grindings) at 900 °C for 5 h under flowing oxygen. The mixture contained a 3 wt % excess of Ag_2O to compensate for loss of Ag during heating. $AgTaO_3$ samples, used as references, were prepared by heating a mixture of Ag_2O and Ta_2O_5 between 850 and 900 °C for 5 h under oxygen flow; a similar 3 wt % excess Ag_2O was used. In all cases, the pellets were placed on a bed of sacrificial powder and covered with a ZrO_2 crucible. A separate Pt container filled with Ag_2O powder was placed inside this crucible next to the sample to provide a silver-oxide-rich atmosphere, during the reaction.

The resulting $AgNb_{1/2}Ta_{1/2}O_3$ powder (light yellow-gray) contained a single perovskite phase as confirmed by X-ray diffraction. The $AgTaO_3$ (light gray) samples contained two perovskite phases: a rhombohedral phase, consistent with the $R\bar{3}c$ structure reported from previous single-crystal studies, and a pseudocubic phase exhibiting broad symmetric peaks in X-ray diffraction (Figure 3). Attempts to isolate a single perovskite AgTaO3 phase by varying the heat-treatment conditions were unsuccessful. The minimal fraction of the pseudocubic phase was obtained using a single heating at 850 °C. [Higher annealing temperatures (i.e., 900 °C) and multiple heat treatments increased the fraction of the pseudocubic phase and eventually led to formation of trace amounts of $Ag_2Ta_4O_{11}$.] The amount of this phase was larger on the surface of the reaction pellet than in the interior; it is likely Ag-deficient and forms as a result of Ag volatility. $AgTaO_3$ samples for structural characterization were prepared from the pellet interiors.

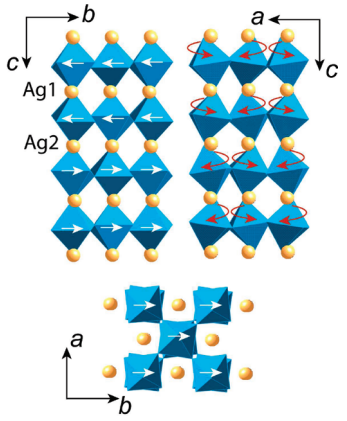

Figure 2. Schematic rendering of the $AgNbO_3$ M-phase structure. White arrows indicate Nb displacements. Red arrows indicate tilting of $[NbO_6]$ octahedra around the *c*-axis.

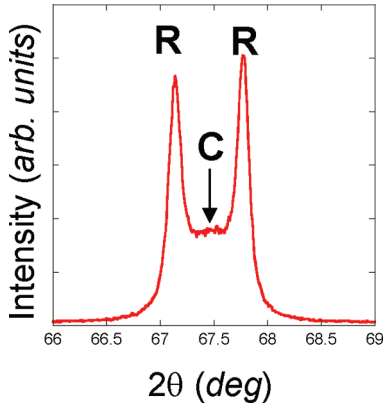

Figure 3. Portion of the X-ray diffraction pattern for $AgTaO_3$ synthesized at 850 °C. The rhombohedral (R) and the pseudocubic (C) peaks are indicated.

(9) Shannon, R. D. *J. Appl. Phys.* **1993**, *73*(1), 348–366.
(10) Borisevich, A. Y.; Davies, P. K. *J. Am. Ceram. Soc.* **2002**, *85*(10), 2487–2491.
(11) Vanderah, T. A.; Collins, T. R.; Wong-Ng, W.; Levin, I.; Roth, R. S.; Farber, L. *J. Alloys Cmpds.* **2002**, *346*(1−2), 116–128.
(12) Kagata, H.; Kato, J. *Jpn. J. Appl. Phys.* **1994**, *33*, 5463.

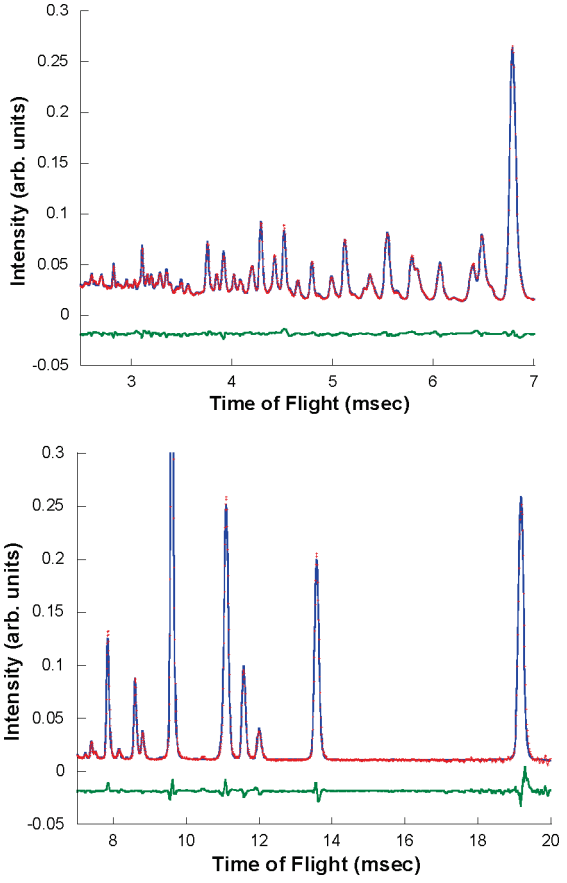

Figure 4. Experimental (crosses) and calculated (line) neutron diffraction profiles for $AgNb_{1/2}Ta_{1/2}O_3$ at room temperature collected using GEM. The calculated profile corresponds to the lattice parameters and atomic positions listed in Table 1.

Variable-temperature (−170 to 450 °C) X-ray diffraction data were collected using a Panalytical Xpert Pro powder diffractometer equipped with an incident beam monochromator ($CuK_{\alpha 1}$ radiation), Pixcel position sensitive detector, and Anton Paar HTK-450 temperature stage. [The use of brand or trade names does not imply endorsement of the product by NIST.] The measurements were conducted in vacuum and the sample powder was mixed with a small amount of a vacuum grease to improve thermal conductivity.

Neutron total scattering measurements on $AgNb_{1/2}Ta_{1/2}O_3$ at room temperature were conducted using the GEM powder diffractometer at ISIS (Rutherford Appleton Laboratory). The data were processed and normalized using the PDFGetN software to deduce atomic pair-distribution functions. Variable-temperature (100−800 K) neutron diffraction data for Rietveld refinements were collected with the HIPD diffractometer at the Lujan Center for Neutron Scattering (Los Alamos National Laboratory); temperature control was achieved using a top-loading displex. In all cases, the sample powders were loaded in vanadium containers. The GSAS software package[13] was used for structural refinements. Three and six detector banks were included in the refinements using data collected on GEM and HIPD instruments, respectively.

Transmission electron microscopy was performed in a Philips CM30 instrument operated at 200 kV and equipped with a Gatan double-tilt heating stage. The samples for TEM were prepared using conventional mechanical polishing and dimpling followed by ion thinning as described in ref 7.

Variable-temperature Nb, Ta, and Ag K-edge EXAFS measurements were conducted at the NIST X23A2 beamline of the National Synchrotron Light Source. The double-crystal monochromator was operated with a pair of Si (311) crystals. Data were collected in transmission using the Linkam heating stage; for these measurements, the sample powder was dispersed in ethanol and mounted on a thin Al foil. All spectra were processed using Athena code.[14] Local-structure refinements were accomplished using the Artemis software.[14] The EXAFS signal was calculated using a self-consistent potential as implemented in the FEFF8.20 code.[15]

Unpolarized Raman spectra were recorded in a backscattering geometry using a Renishaw RM 1000 micro-Raman spectrometer equipped with a grating cutoff filter (NExT). The 514.5 nm line of an Ar laser was used for excitation; laser power of ~10 mW was focused into a 2 μm spot on the sample surface. A Linkam THMS 600 stage was used for temperature control. The spectra were processed and fitted using custom computer software.

Table 1. Room-Temperature Atomic Coordinates and Isotropic Displacements Parameters (Å^2) for the *Pbcm* Structure of $AgNb_{1/2}Ta_{1/2}O_3$ Obtained from Refinements Using Neutron Powder Diffraction Data (Figure 4)[a]

atom	site	x	y	z	$U_{iso} \times 100$
Ag1	4*d*	0.7561(8)	0.2413(5)	0.75	1.18(4)
Ag2	4*c*	0.7529(8)	0.25	0.50	0.89(3)
Nb	8*e*	0.7483(3)	0.7409(2)	0.6239(2)	0.52(1)
O4	4*d*	0.7134(4)	0.7608(5)	0.75	0.419(4)
O5	4*c*	0.8174(4)	0.75	0.5	0.34(4)
O6	8*e*	0.4731(3)	0.5277(4)	0.6103(1)	0.77(3)
O7	8*e*	0.9687(3)	0.4692(4)	0.6376(1)	0.992(3)

[a] Lattice parameters a = 5.5238(1) Å, b = 5.5673(1) Å, c = 15.6721(4) Å. Space group *Pbcm* (No. 57).

Results and Discussion

Room-Temperature Structure. X-ray and neutron powder diffraction patterns for $AgNb_{1/2}Ta_{1/2}O_3$ can be indexed according to the unit cell of $AgNbO_3$ with lattice parameters (X-ray) a = 5.5371(1) Å, b = 5.5794(1) Å, c = 15.7104(2) Å. The experimental and calculated neutron diffraction profiles are shown in Figure 4 (GEM data). Table 1 summarizes atomic coordinates and atomic displacement parameters (ADP) as refined using these data (isotropic ADP values were assumed). The atomic parameters refined using the GEM and HIPD data agreed within ±2 e.s.d. values.

Electron diffraction data (Figure 5) confirm *Pbcm* symmetry for $AgNb_{1/2}Ta_{1/2}O_3$, as evidenced from reflection conditions because of the symmetry glide-planes. The diffraction patterns of $AgTaO_3$ are consistent with the previously reported rhombohedral $R\bar{3}c$ structure associated with $a^-a^-a^-$ tilting; however, pronounced diffuse $\langle 100 \rangle_c$ rods of intensity passing through $^1/_2hkl_c$ (h,k,l = odd) reflections reveal partial tilting disorder that indicates local deviations from rhombohedral symmetry. Like $AgNbO_3$, $AgNb_{1/2}Ta_{1/2}O_3$ exhibits sheets of diffuse

(13) Larson, A. C.; van Dreele, R. B. LAUR Report No. 86-748. Unpublished work, **1994**.

(14) Ravel, B.; Newville, M. *J. Synchrotron Radiat.* **2005**, *12*, 537.
(15) Zabinsky, S. I.; Rehr, J. J.; Ankudinov, A.; Albers, R. C.; Eller, M. J. *Phys. Rev. B* **1995**, *52*, 2995.

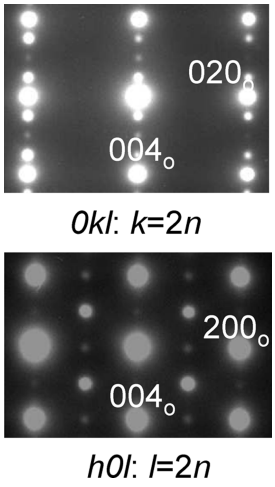

Figure 5. Electron diffraction patterns recorded from the single domain of $AgNb_{1/2}Ta_{1/2}O_3$ at room-temperature. The reflection conditions resulting from the symmetry glide-planes in *Pbcm* space group are indicated.

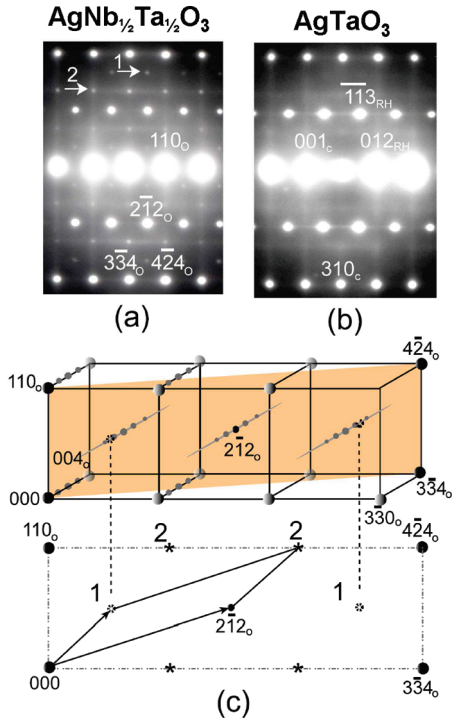

Figure 6. Electron diffraction patterns recorded from (a) $AgNb_{1/2}Ta_{1/2}O_3$ and (b) $AgTaO_3$ in $[310]_c$ zone axis orientations. The reflections are indexed according to the orthorhombic ($\sqrt{2}a_c \times \sqrt{2}a_c \times 4a_c$) and rhombohedral ($\sqrt{2}a_c$, $\alpha \approx 60°$, hexagonal setting, 3 axis system) unit cells of these two compounds, respectively; the indexes corresponding to the ideal cubic perovskite cell are indicated as well. The traces of diffuse scattering passing through fundamental reflections arise from diffuse scattering sheets perpendicular to orthogonal [100] directions. The diffraction pattern for $AgTaO_3$ exhibits additional pronounced diffuse streaks passing through the $1/2hkl$ (h, k, l = odd) superlattice reflections which reflect tilting disorder. The diffraction pattern for $AgNb_{1/2}Ta_{1/2}O_3$ exhibits weak extra spots, numbered 1 and 2, which should be absent for the $\sqrt{2}a_c \times \sqrt{2}a_c \times 4a_c$ lattice. The origin of these spots is illustrated schematically in c. The type 1 spots arise from the intersection of $[001]_o$ rods of intensity passing through the $2\bar{1}2_o$-like reflections with the $2\bar{2}3_o$-like plane of the diffraction pattern, as confirmed by tilting experiments. The type 2 spots are attributed to multiple scattering that involves both type 1 and $2\bar{1}2_o$-like reflections.

intensity passing through all fundamental reflections parallel to the three orthogonal sets of $\{100\}_c$ planes. Similar sheets

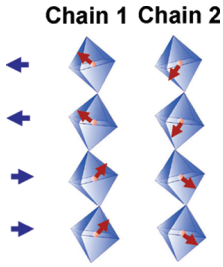

Figure 7. Schematic drawing illustrating B-cation displacement (red arrows) correlations giving rise to {001} diffuse scattering sheets in electron diffraction patterns of $AgNbO_3$.[7] The sample represents a random mixture of the two types of octahedral chains. The correlations in the M-structure of $AgNbO_3$-based ceramics are more complex than those in $KNbO_3$[16] to conform to the average antipolar ordering on the B-sites (indicated using arrows on the left).

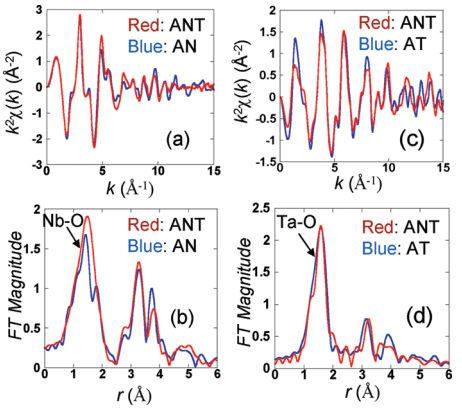

Figure 8. (a) EXAFS data (b) magnitude of EXAFS Fourier transform (FT) for Nb in $AgNb_{1/2}Ta_{1/2}O_3$ (ANT, red) and $AgNbO_3$ (AN, blue); (c) EXAFS data and (d) magnitude of EXAFS FT for Ta in $AgNb_{1/2}Ta_{1/2}O_3$ (red) and $AgTaO_3$ (blue). The k-ranges used in the Fourier transforms were 2.5−14.2 $Å^{-1}$ for Nb and 2.05−14.0 $Å^{-1}$ for Ta.

of diffuse intensity were encountered in $AgTaO_3$ (Figure 6). This type of diffuse scattering has been attributed to the local off-center B-cation displacements along the $\langle 111\rangle_c$ directions. According to the existing model,[7,16] the $\langle 100\rangle_c$ components of these displacements are correlated along the −B−O−B− chains yielding corresponding diffuse planes in reciprocal space (Figure 7). Our present results suggest that such local correlated displacements exist across the entire $AgNbO_3$−$AgTaO_3$ system.

EXAFS analyses for Nb and Ta in $AgNb_{1/2}Ta_{1/2}O_3$ reveal different distortions of the oxygen coordination environment for the two cations. Fitting the first B−O peak in EXAFS yields R_{Nb-O} = 1.99(1) Å, σ^2_{Nb-O} = 0.011(1) $Å^2$, R_{Ta-O} = 1.96(1) Å, σ^2_{Ta-O} = 0.006(1) $Å^2$. Clearly, the Nb−O environment is more distorted than that of Ta−O, as evident from the significantly larger Debye−Waller (D−W) factor (i.e., σ^2) for the Nb−O distances. These results can be attributed to the larger off-center displacements of Nb. Figure 8 compares Nb and Ta EXAFS in $AgNb_{1/2}Ta_{1/2}O_3$ to the data collected on $AgNbO_3$ and $AgTaO_3$, respectively. In $AgNbO_3$, fitting the Nb−O peak required two distinct distances of 1.905 and 2.10 Å (σ^2_{Nb-O} = 0.005 $Å^2$). In $AgNb_{1/2}Ta_{1/2}O_3$, this splitting appears to be reduced while

(16) Comes, R.; Lambert, M.; Guinier, A. *Solid State Commun.* **1968**, *6*, 715.

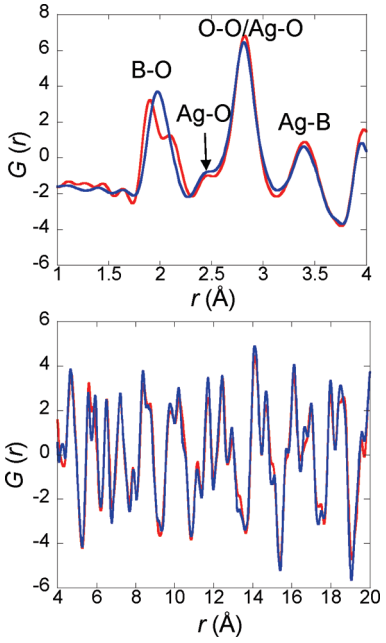

Figure 9. Neutron pair-distribution functions for $AgNb_{1/2}Ta_{1/2}O_3$ (blue) and $AgNbO_3$ (red). Both PDFs were obtained using $Q_{max} \approx 35$ Å^{-1}. The B−O distance distribution in $AgNb_{1/2}Ta_{1/2}O_3$ is significantly narrower than that in $AgNbO_3$.

still being manifested in the relatively large D−W factor (0.01 Å^2). In contrast, the Ta−O distance and its associated D−W factor are similar for $AgNb_{1/2}Ta_{1/2}O_3$ and $AgTaO_3$.

A pair-distribution function (PDF) obtained from the total neutron scattering exhibits a single B−O peak as opposed to a well-resolved doublet for $AgNbO_3$, as expected for the superposed Nb−O and Ta−O distances (Figure 9). [Neutron scattering lengths of Nb (7.054 fm) and Ta (6.91 fm) are close to each other which makes these elements effectively indistinguishable for neutron diffraction.] This PDF can be fitted satisfactorily in the entire *r*-range using the average structure model. The overall spread of the B−O distances in $AgNb_{1/2}Ta_{1/2}O_3$ is significantly narrower compared to that of $AgNbO_3$, consistent with a smaller distortion of the Nb−O environment suggested by EXAFS. This result is in contrast to solid solutions that combine ions having different sizes.

Thus, $AgNb_{1/2}Ta_{1/2}O_3$ at room temperature exhibits a *Pbcm* average structure described by complex tilting of [BO_6] octahedra combined with small off-center cation (Ag, Nb/Ta) displacements directed primarily along the *b*-axis. Diffuse scattering in electron diffraction suggests that the B-cations are locally displaced off center along $\langle 111 \rangle_c$ directions, with the $\langle 100 \rangle_c$ displacement components correlated along the −B−O−B− chains. According to EXAFS, Nb exhibits much larger displacements than Ta though the magnitude of local Nb displacements in $AgNb_{1/2}Ta_{1/2}O_3$ is appreciably smaller compared to those in $AgNbO_3$. Despite the similar nominal ionic radii of Ta and Nb, R_{Ta-O} (1.96 Å) is shorter than R_{Nb-O} (1.99 Å), indicating stronger Ta−O bonds. As a result, Ta substitution for Nb slightly increases the effective perovskite tolerance factor, which is consistent with different types of octahedral tilting exhibited by $AgTaO_3$ ($a^-a^-a^-$) and

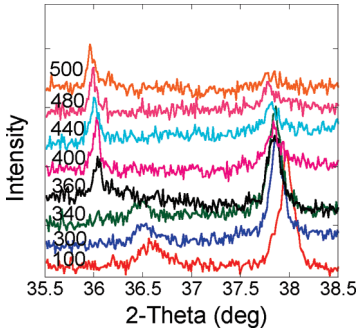

Figure 10. Portions of variable-temperature X-ray diffraction patterns recorded from $AgNb_{1/2}Ta_{1/2}O_3$ which contain the superlattice reflections associated with *in-phase* ($2\theta \approx 36°$) and *antiphase* ($2\theta \approx 38°$) octahedral tilting. The reflection at $2\theta \approx 36.5°$ is characteristic of the *Pbcm* M_3/M_2 structure. The temperatures (°C) are indicated in the plot (the data were collected every 10 °C, but only the representative scans are shown for clarity). The changes in the intensities of the tilting reflections across the M ↔ O (~350 °C) and O ↔ T (~350 °C) transitions can be observed.

$AgNbO_3$ ($[a^-a^-c^-]/[a^-a^-c^+]$). The shorter Ta−O bond and smaller off-center displacements of Ta are also consistent with smaller dielectric constants exhibited by tantalates compared to niobates, as well as with different values of the effective electronegativity for Ta and Nb as inferred from diffuse reflectance measurements.[17]

Phase Transitions. *A. Tilting Transitions.* Variable-temperature X-ray diffraction measurements confirm that the M-structure is stable up to ~350 °C and transforms to another orthorhombic phase at higher temperatures, consistent with the previous work.[5,6] According to neutron diffraction studies by Sciau et al.,[6] this orthorhombic structure (O), exhibits $a^0b^+c^-$ tilting giving rise to the $2a_c \times 2a_c \times 2a_c$ orthorhombic unit cell and *Cmcm* symmetry. [The neutron diffraction study[7] could not distinguish between the O_1 and O_2 phases suggested by the phase diagram, which was based on X-ray diffraction.[5]] Our X-ray diffraction data for the O phase confirm the presence of superlattice reflections because of both *in-phase* and *antiphase* tilting, which are consistent with the *Cmcm* structure (Figure 10). Subsequent heating of the O phase to higher temperatures results in the disappearance of the antiphase tilting reflections at ~480 °C, but the in-phase tilting is preserved, as expected for the reported phase transition from O to the tetragonal (T) structure with $a^0a^0c^+$ tilting (*P4/mbm* symmetry). The splitting of fundamental reflections in the X-ray diffraction patterns is also consistent with the tetragonal unit cell. The T-phase transforms to the ideal cubic perovskite structure at ~540 °C, in agreement with the phase diagram (Figure 1).

In situ electron diffraction measurements confirm that the *Pbcm* phase is first replaced by a structure that combines antiphase and in-phase tilts (e.g., $a^0b^+c^-$) (Figure 11). The transition sequence is inferred from the changes in the intensity and appearance of the $^1/_2hk0_c$ (h,k = odd) and $^1/_2hkl_c$ (h,k,l = odd) superlattice reflections. In the *Pbcm* phase, the $^1/_2hk0_c$ reflections (e.g., $^1/_2310_c$) are

(17) Eng, H. W.; Barnes, P. W.; Auer, B. M.; Woodward, P. M. *J. Solid State Chem.* **2003**, *175*, 94–109.

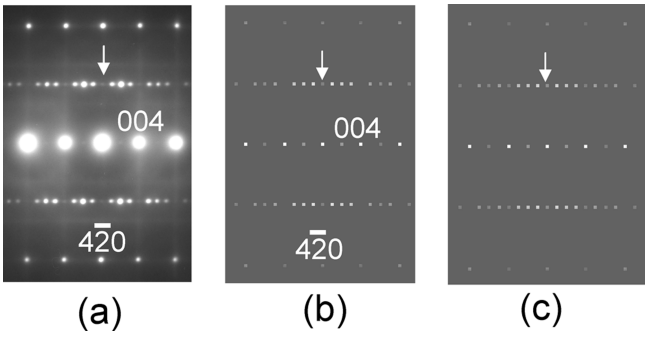

Figure 11. (a) Experimental and (b, c) calculated electron diffraction patterns for $AgNb_{1/2}Ta_{1/2}O_3$ in the $[120]_o||\langle 310\rangle_c$ zone axis orientation. The calculated pattern (b) corresponds to the refined structural model (Table 1). The pattern was calculated using the Bloch-waves formalism for a typical sample thickness of 20 nm (the calculations performed for a series of thicknesses yielded similar results). The calculated intensities are displayed on a logarithmic scale. Note very weak intensities of the $2\bar{1}0_o$-type reflections, similar to those observed in the experimental pattern (a). Likewise, the calculations reproduce the pseudoextinctions of superlattice reflections along the *c*-axis rows containing $4\bar{2}0_o$-type reflections. The calculated pattern (c) corresponds to a model with the artificially enhanced Nb/Ta displacements. The $2\bar{1}0_o$-type reflections in this pattern are significantly stronger compared to those in b.

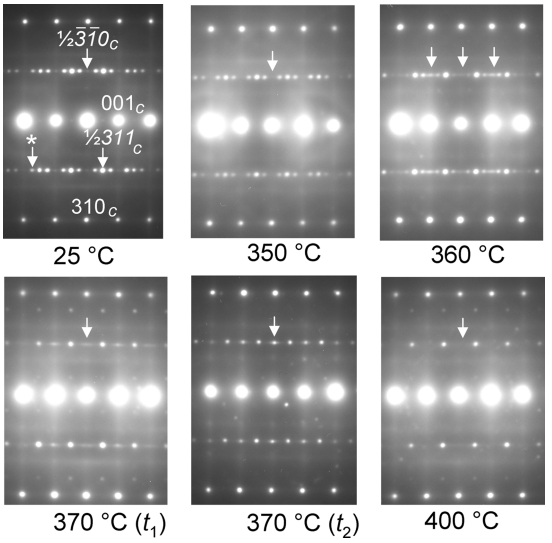

Figure 12. Variable-temperature electron diffraction patterns recorded $AgNb_{1/2}Ta_{1/2}O_3$ in the $\langle 310\rangle_c$ zone axis orientation. Changes in the intensities of $^1/_2310_c$, $^1/_2311_c$, and $^1/_400l_c$-type (indicated using asterisk) reflections signify tilting phase transitions as described in the text. t_1 and t_2 indicate different times.

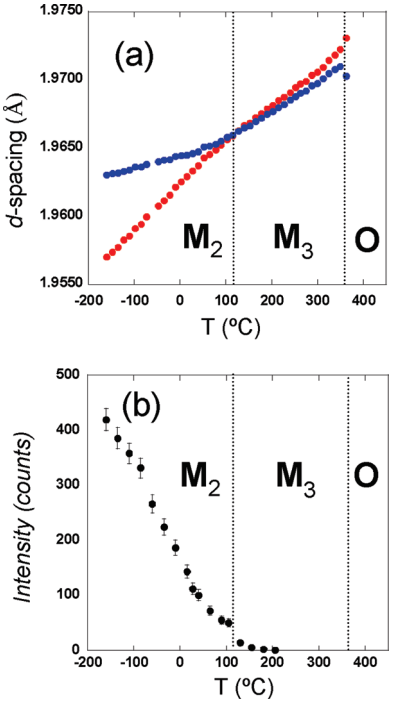

Figure 13. Temperature dependence for the 220_o and 008_o *d*-spacings in $AgNb_{1/2}Ta_{1/2}O_3$. These *d*-spacings were calculated from the lattice parameters obtained using variable-temperature X-ray diffraction data.

determined primarily by the cation (Ag, Nb, Ta) antiparallel displacements, whereas the $^1/_2hkl_c$ (e.g., $^1/_2311_c$) reflections are dominated by antiphase octahedral titling. In $AgNb_{1/2}Ta_{1/2}O_3$, at room temperature, the $^1/_2hk0_c$ reflections are weak because of the small magnitudes of cation displacements as confirmed by Rietveld refinements and simulations of electron diffraction data (Figure 11). Their intensity decreases further on heating until no detectable $^1/_2hk0_c$ maxima can be observed, despite the same *Pbcm* symmetry of the tilted octahedral framework. At ~370 °C (Figure 12), the diffuse intensity condenses again at the $^1/_2hk0_c$ locations eventually yielding discrete, relatively strong $^1/_2hk0_c$ spots with concurrent vanishing of the $^1/_400l_c$-type reflections (indicated using asterisk). These changes are consistent with the M ↔ O transition. The O phase exhibits a combination of *in-phase* and *antiphase* tilts, where the $^1/_2hk0_c$ reflections become dominated by the *in-phase* octahedral rotations. Similar behavior is observed for the $^1/_2hk0_c$ reflections in the X-ray diffraction patterns. Further heating by only 20−30 °C results in another phase transition manifested in the disappearance of the $^1/_2hk0_c$ spots so that only the $^1/_2hkl_c$ reflections associated with antiphase tilting remain. This transition appears to be in contrast to the X-ray diffraction data which suggests that O transforms into the tetragonal structure (T) featuring in-phase rather than antiphase tilting. Unfortunately, more detailed studies of the high-temperature phases in electron diffraction were precluded by precipitation of metallic Ag, a common problem in high-temperature TEM studies of $AgNbO_3$-based ceramics. Conceivably, the discrepancy between the electron and X-ray diffraction data is caused by the onset of the decomposition of $AgNb_{1/2}Ta_{1/2}O_3$ at high-temperatures in TEM, since the resulting Ag deficiency can stabilize a different type of octahedral tilting.

B. Displacive Cation Disorder−Order Transitions. Similar to $AgNbO_3$, the splitting of the 220_o (subscript o refers to the orthorhombic unit cell $\sqrt{2}a_c \times \sqrt{2}a_c \times 4a_c$) and 008_o reflections remains very small in the entire M_3 field but increases abruptly below the $M_3 \leftrightarrow M_2$ transition at ~120 °C (Figure 13a). Concurrently, the intensity of the 313_o superlattice reflection, determined primarily by the magnitudes of cation displacements, remains weak in the M_3 structure but increases markedly below the $M_3 \leftrightarrow M_2$ transition (Figure 13b). By analogy with $AgNbO_3$, this drastic change in the slope of temperature dependence for the 313_o reflection is attributed to the ordering of local

Table 2. Nb−O (R_{Nb-O}) and Ta−O (R_{Ta-O}) Distances and Their Associated Debye−Waller (σ^2) Factors in $AgNb_{1/2}Ta_{1/2}O_3$ as Determined from Fitting the First Peak in Nb and Ta EXAFS FT, Respectively[a]

temperature (°C)	R_{Nb-O} (Å)	σ^2_{Nb-O} (Å^2)	R_{Ta-O} (Å)	σ^2_{Ta-O} (Å^2)
25	1.99(1)	0.011(2)	1.96(1)	0.006(1)
−173	1.92(2)+2.07(2)	0.006(3)	1.96(1)	0.006(1)

[a] The numbers in parentheses represent uncertainties as estimated by Artemis/IFEFFIT.[14]

cation displacements within *Pbcm* symmetry. In $AgNb_{1/2}Ta_{1/2}O_3$, the onset of cation ordering is suppressed down to much lower temperatures relative to the temperature of the tilting $M_3 \leftrightarrow O$ transition ($\Delta T \approx 250$ °C) as compared to $AgNbO_3$ ($\Delta T \approx 75$ °C).

Comparison of EXAFS data collected at 25 and −173 °C indicates the absence of significant changes in the Nb−O and Ta−O distances, except for a somewhat larger splitting of the short and long Nb−O distances at lower temperatures (Table 2). The diffuse scattering in electron diffraction also exhibits no obvious changes with temperature. Unlike $AgNbO_3$, where the $(100)_c$ and $(010)_c$ diffuse sheets disappeared below ~200 °C leaving only the $(001)_c$ sheets intact, in $AgNb_{1/2}Ta_{1/2}O_3$, all three sets of orthogonal $\{100\}_c$ diffuse sheets remained visible down to −173 °C, which was the lowest temperature attainable with the presently used sample holder. Possible contributions of diffuse sheets from the twin domains were eliminated by using the $\langle 130\rangle_c$ orientation that does not contain the *c*-axis. These results suggest a larger degree of residual displacive disorder in the M_2 phase of $AgNb_{1/2}Ta_{1/2}O_3$ compared to $AgNbO_3$.

Neutron powder diffraction data collected for $AgNb_{1/2}Ta_{1/2}O_3$ in the temperature range from −173 °C to +340 °C (the maximum temperature attainable with the top-loading displex used) were successfully fitted using the *Pbcm* structure. The angles of octahedral rotations around the *c*- (ϕ) and *b*-axes (θ), calculated from the oxygen coordinates, increase monotonically with decreasing temperature (Figure 14a); the magnitudes in $AgNb_{1/2}Ta_{1/2}O_3$ are slightly (~0.5°) smaller than those for the corresponding temperatures in $AgNbO_3$. These differences are reproducible for the data collected on the GEM and HIPD instruments and are significant with respect to the estimated standard deviations in the refined oxygen coordinates. Smaller tilting angles in $AgNb_{1/2}Ta_{1/2}O_3$ are consistent with a larger value of the tolerance factor (i.e., closer to the ideal value of 1) compared to $AgNbO_3$ because of a smaller size of the [TaO_6] octahedra.

Temperature dependencies of the *b*-axis displacements for Nb/Ta and Ag1 from their ideal cubic positions are summarized in Figure 14b and c, respectively. The magnitudes of these displacements remain suppressed over a relatively broad temperature range down to 150 °C but increase progressively on cooling below this temperature, consistent with X-ray diffraction data (Figure 13b). This onset of significant *average* displacements can be attributed to a partial ordering of Nb and, possibly, Ag over their *local* off-centered positions. The average cation displacements in $AgNb_{1/2}Ta_{1/2}O_3$ appear to be appreciably (~3 times for Nb/Ta and up to ~6 times for Ag1) smaller than the corresponding values in $AgNbO_3$. These differences cannot be accounted for by a mixture of displaced Nb and centered Ta in $AgNb_{1/2}Ta_{1/2}O_3$ but likely reflect a weaker ordering of local displacements in the solid-solution structure as compared to the end-compound. This interpretation concurs with the observed diffuse scattering in electron diffraction, which revealed the presence of three sets of diffuse $\{001\}_c$ sheets down to −173 °C in $AgNb_{1/2}Ta_{1/2}O_3$, as opposed to a single set observed for $AgNbO_3$ below 200 °C.

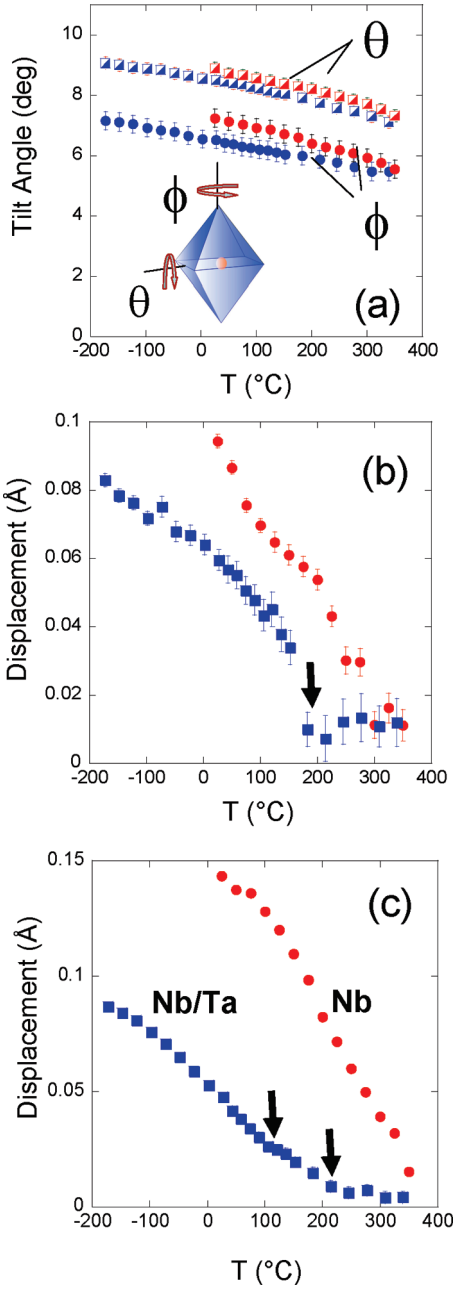

Figure 14. Temperature dependencies of (a) octahedra tilting angles and magnitudes of the *b*-axis (b) Ag1 and (c) Nb displacements in $AgNb_{1/2}Ta_{1/2}O_3$ and $AgNbO_3$ obtained from Rietveld refinements using variable-temperature neutron powder diffraction data. These characteristics were calculated from the presently refined atomic coordinates for $AgNb_{1/2}Ta_{1/2}O_3$ and from the structural data for $AgNbO_3$ reported in ref 7.

Previous work on $AgNbO_3$ assumed that the displacive disorder is primarily associated with Nb, though some

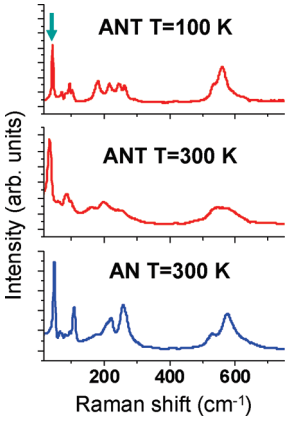

Figure 15. Representative Raman spectra of $AgNbO_3$ (AN) and $AgNb_{1/2}Ta_{1/2}O_3$ (ANT).

indications of similar behavior on the Ag sites was observed as well.[7] Reverse Monte Carlo (RMC) refinements of local structure in $AgNbO_3$ using a combined input from neutron/X-ray total scattering and EXAFS suggested 2-site disorder for both Ag1 (site splitting along the *c*-axis) and Ag2 (split along the *b*-axis).[18] A-cation displacements in perovskites are commonly coupled to octahedral rotations, which are driven by under-bonded A-cations. Much smaller magnitudes of Ag displacements in $AgNb_{1/2}Ta_{1/2}O_3$ compared to those in $AgNbO_3$ contrast with the relatively similar tilting angles in the two structures. One explanation for this apparent discrepancy involves partial ordering of Ag over the off-centered split sites, similar to the B-cations. In that case, the average Ag displacements represent an order parameter and are different from the local displacements, which can be significantly larger. Unfortunately, analyses of Ag EXAFS are ineffective for the determination of local Ag displacements because the distortion of the Ag−O environment is defined primarily by octahedral tilting (i.e., oxygen displacements), and the magnitudes of Ag displacements off their ideal cubic positions are small (<0.05 Å).

Overall, our results indicate that the onset of ordering for the local cation displacements in $AgNb_{1/2}Ta_{1/2}O_3$ is strongly suppressed, presumably because of the dissimilar tendencies for off-center displacements for Nb and Ta. The results obtained for $AgNb_{1/2}Ta_{1/2}O_3$ demonstrate the likelihood of displacive ordering for Ag, in addition to that observed for the B-cations; as expected, the displacements on the A- and B-sites appear to be coupled. Ordering of the B-cation displacements is accompanied by distortions of oxygen octahedra (compression along the *c*-axis and expansion in the *ab*-plane), which are manifested in the splitting of the 220_o and 008_o reflections.

Raman Spectra. Raman spectra of $AgNbO_3$ and $AgNb_{1/2}Ta_{1/2}O_3$ are compared in Figure 15. The spectrum of $AgNbO_3$ contains multiple peaks that, as suggested previously,[19] can be grouped into the low- (<120 cm^{-1}), intermediate- (120−350 cm^{-1}) and high-frequency (>450 cm^{-1}) bands. By analogy with $KNbO_3$,[20] the high- and the intermediate-frequency regions have been attributed to the split cubic highest-frequency F_{1u} and the intermediate-frequency F_{2u}, and F_{1u} phonon bands. The suggested origins for the low-frequency part of the spectrum include the split cubic lowest-frequency F_{1u} mode and the phonon branches activated by the structural phase transitions. Visual inspection of the Raman spectra collected across the phase transitions reveals no abrupt changes at the transition temperatures. Previous reports[21] suggested that both the lowest-frequency peak (~50 cm^{-1}) and the quasi-elastic central scattering display distinct changes at the $M_3 \leftrightarrow M_2$ transition. This transition is manifested in the marked softening of the lowest-frequency peak accompanied by the concurrent increase in the diffusion of the central peak; this diffusion is maximal at the $M_3 \leftrightarrow M_2$ transition temperature. However, no obvious changes in other parts of the Raman spectra could be observed.

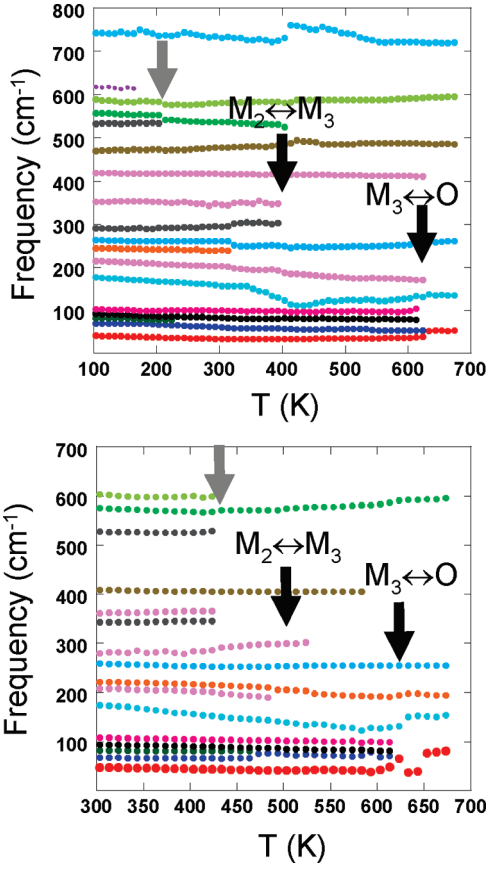

Figure 16. Temperature dependencies of the oscillator frequencies obtained by fitting the Raman spectra for (top) $AgNb_{1/2}Ta_{1/2}O_3$ and (bottom) $AgNbO_3$. The number of oscillators needed to fit the data changes in the vicinity of phase transitions.

In the present study, we performed fitting of the as-measured Raman spectra using a sum of the peaks representing an ensemble of the damped oscillators. The Bose−Einstein factor was incorporated in the fitting procedure.

(18) Krayzman, V.; Levin, I. J. Phys. Cond. Matter **2010**, in press.
(19) Kania, A.; Roleder, K.; Kugel, G. E.; Fontana, M. D. *J. Phys. C: Solid State Phys.* **1986**, *19*, 9–20.
(20) Fontana, M. D.; Ridah, A.; Kugel, G. E.; Carabatos-Nedelec, C. *J. Phys. C: Solid State Phys.* **1988**, *21*, 5853–5879.
(21) Hafid, M.; Kugel, G. E.; Kania, A.; Roleder, K.; Fontana, M. D. *J. Phys. Cond. Matter* **1992**, *4*, 2333–2345.

The central feature was described using a mixture of the Lorentzian and triangular functions. The fitting parameters for each oscillator peak included frequency, amplitude and line width. The number of oscillators was adjusted to obtain the best fit. The temperature dependencies of the refined oscillator frequencies in $AgNbO_3$ and $AgNb_{1/2}Ta_{1/2}O_3$ are summarized in Figure 16. In both systems, the number of oscillators changes near the temperatures of the $O \leftrightarrow M_3$ and $M_3 \leftrightarrow M_2$ transitions. Additional changes in the number of oscillators at 425 K for $AgNbO_3$ and 200 K for $AgNb_{1/2}Ta_{1/2}O_3$ may reflect further displacive ordering for Nb and Ag. These results indicate that despite lack of changes in the average symmetry, the displacive cation ordering does affect all parts of the phonon spectra for both $AgNbO_3$ and $AgNb_{1/2}Ta_{1/2}O_3$.

Conclusions

The structure of the M-phase in $AgNb_{1/2}Ta_{1/2}O_3$ is similar to that in $AgNbO_3$. According to EXAFS measurements, Nb cations exhibit significantly larger off-center displacements than Ta. This disparity in the magnitudes of Nb and Ta displacements is maximal for $AgNbO_3$ and $AgTaO_3$ but significantly reduced in $AgNb_{1/2}Ta_{1/2}O_3$; therefore, the solid solution structure exhibits smaller local distortions than the end-compound. Similar to $AgNbO_3$, the $M_3 \leftrightarrow M_2$ transition in $AgNb_{1/2}Ta_{1/2}O_3$ is accompanied by ordering of local B-cation displacements that exhibit 8-site disorder at higher temperatures. However, Ta substitution suppresses this ordering because of the different off-centering trends for Nb and Ta. Despite similar tilting angles in the M_2-structures of $AgNb_{1/2}Ta_{1/2}O_3$ and $AgNbO_3$, the magnitudes of the average B-cation and Ag displacements in the solid solution are much smaller compared to those in $AgNbO_3$. Comparison of the temperature dependencies for the tilting angles and the magnitudes of the average off-center Ag displacements suggests displacive ordering of Ag coupled to the ordering of the B-cations. The presence of the three orthogonal sets of $\{100\}_c$ diffuse sheets in the electron diffraction patterns of $AgNb_{1/2}Ta_{1/2}O_3$ down to low temperatures indicate the existence of residual 8-site disorder on the B-sites in the partially ordered M_2 structure, which contrasts with 2-site disorder in the M_2 structure of $AgNbO_3$. Detailed analyses of variable-temperature Raman spectra reveal qualitative changes in the phonon spectra of both $AgNbO_3$ and $AgNb_{1/2}Ta_{1/2}O_3$ in the vicinity of the displacive cation ordering transitions within the M-phase field. The Ta−O bond length is shorter than the average Nb−O bond length which, along with a stronger off-centering of Nb, is consistent with the larger dielectric constants typically exhibited by niobates compared to tantalates.

Acknowledgment. Neutron diffraction measurements were conducted at (1) the Lujan Center at Los Alamos Neutron Science Center funded by the Department of Energy Office of Basic Energy Sciences and Los Alamos National Laboratory under contract No. W-7405-ENG-36 and (2) the ISIS Pulsed Neutron and Muon Source supported by a beam-time allocation from the Science and Technology Facilities Council.